PERGAMON

Chemical
Engineering Science

Natural gas production from hydrate decomposition by depressurization

Chuang Ji[a,b], Goodarz Ahmadi[a,b], Duane H. Smith[a,*]

[a] *National Energy Technology Laboratory, US Department of Energy, Morgantown, WV 26507-0880, USA*
[b] *Department of Mechanical and Aeronautical Engineering, Clarkson University, Potsdam, NY 13699-5725, USA*

Received 10 March 2000; received in revised form 23 October 2000; accepted 24 April 2001

Abstract

This paper presents a parametric study of natural gas production from the decomposition of methane hydrate in a confined reservoir by a depressurizing well. The one-dimensional linearized model suggested by Makogon is used in the analysis. For different well pressures and reservoir temperatures, distributions of temperature and pressure in the porous layer of methane hydrate and in the gas region are evaluated. The distance of the decomposition front from the well and the natural gas output as functions of time are also computed. Time evolutions of the resulting temperature and pressure profiles in the hydrate reservoir under various conditions are presented. Effects of variations in reservoir porosity and zone permeability are also studied. It is shown that the gas production rate is a sensitive function of well pressure, reservoir temperature and zone permeability.

Keywords: Hydrate dissociation; Natural gas production; Depressurizing well; Hydrate reservoir

1. Introduction

Natural gas hydrates are solid molecular compounds of water with natural gas that are formed under certain thermodynamic conditions. World reserves of natural gas trapped in the hydrate state have been estimated to be several times the known reserves of conventional natural gas (Makogon, 1997). Therefore, developing methods for commercial production of natural gas from hydrates is attracting considerable attention.

All known methods of decomposition of hydrates are based on shifting the thermodynamic equilibrium in a three-phase system (water–hydrate–gas), which can be achieved by

- increasing the system temperature above the temperature of hydrate formation at a specified pressure;
- decreasing the system pressure below the pressure of hydrate formation at a specified temperature; or
- injecting inhibitors such as methanol to shift the pressure–temperature equilibrium.

The case that a well is drilled into a hydrate reservoir and initiates a depressurization is considered in this study.

Extensive reviews of hydrate formation and decomposition processes were reported by Makogon (1997) and Sloan (1998). Thermodynamic modeling of the hydrate decomposition process by depressurization has been studied by a number of authors. Assuming that the process of hydrate decomposition by a pressure decrease is analogous to the process of solid melting, Makogon (1974, 1997) used the classical Stefan's problem for melting to describe the process of hydrate decomposition. The linearized governing equations for the movement of natural gas in a porous medium coupled with heat transfer were solved, and self-similar solutions for the pressure distributions were obtained. The release of water during the hydrate decomposition, however, was neglected in this model.

Verigin, Khabibullin, and Khalikov (1980) considered the effect of water flow and developed a more accurate model. In this model the gas and water mass balance at

* Corresponding author. Tel.: +1-304-285-4799; fax: +1-304-285-4469.
E-mail address: dsmith@netl.doe.gov (D. H. Smith).

the surface of decomposition were considered separately. The water produced from the hydrate dissociation was assumed to be stationary and not to affect the flow of natural gas. The change of temperature of the hydrate layer during the movement of natural gas, however, was not considered in these earlier models.

Holder, Angert, and Godbole (1982) considered the variation of temperature during the hydrate decomposition in their study. They used the conduction heat transfer equation for evaluating the temperature distribution in a hydrate layer. The continuity equation was used to describe the natural gas flow, in which the pressure gradient and the gas flow velocity were connected by Darcy's law. An empirical formula was used to calculate the dissociation enthalpy for hydrates. The movement velocity of the surface of decomposition, which reflected the rate of hydrate dissociation at the surface, was determined by the magnitude of the dissociation enthalpy and the temperature gradient in the hydrate layer.

Burshears, O'Brien, and Malone (1986) extended the model of Holder et al. (1982) and considered the influence of water transport in the layer, in addition to the natural gas flow. They also included the effect of water that is produced by the dissociated hydrate. However, the connective heat transfer in the area where gas and water coexist was not considered. Selim and Sloan (1989) considered the convective-conductive heat transfer in their one-dimensional model. Under the assumption that the water in the reservoir remained motionless and the well temperature was kept constant, they obtained an analytical expression for the temperature distribution in the reservoir.

Kamath (1983) used a modified Clausius–Clapeyron equation to obtain the enthalpy of dissociation for hydrates of different gases. He studied the process of hydrate dissociation by heating. Hot water was used in the experiment, and the results showed that the rate of heat transfer and the rate of hydrate dissociation were power law functions of the temperature difference. This research also revealed additional details about the process of heat transfer at the hydrate dissociation interface. Recent studies on geological aspects of hydrates were reported in AGU (1999).

Makogon (1997) summarized the study of Bondarev and Cherskiy, where the effects of heat transfer in the porous medium were included. The energy equation was used to describe the thermal condition of natural gas in the porous layer. The conductive and convective heat transfer, as well as the effects of the throttling process were included. Makogon (1997) reported analytical expressions for the one-dimensional temperature and pressure profiles that were obtained after linearization of the governing equations.

Lysne (1994) studied the water and gas flows during the dissociation of hydrate in a pipe. Tsypkin (2000) also described the movement of water and gas in the reservoir using a multiphase one-dimensional model. He obtained similarity solutions for temperature and pressure distributions by a perturbation method. Masuda et al. (1999) treated the process of hydrate dissociation as a Kim, Bishnoi, Heidemann, and Rizvi (1987) kinetic process. In this model the rate of dissociation is related to the difference between the equilibrium pressure and gas pressure. Their numerical results were in agreement with their experimental data. Moridis, Apps, Pruess, and Myer (1998) added a module for hydrate dissociation into the TOUGH2 general-purpose reservoir simulator. The flow of gas and water were considered and the conductive–convective heat transfer equation was used.

Durgut and Parlaktuna (1996) simulated natural gas production by hot water injection into the hydrate reservoir. Their developed two-dimensional model included heat conduction and convection, and both water and gas flows. More recently Swinkels and Drenth (1999) studied the behavior of a hydrate-capped gas reservoir using a three-dimensional thermal reservoir simulator. They concluded that the simulation could provide insight into the process and for economical evaluation of production scenarios. They also noted that the gas production from the hydrate cap might become thermally limited.

In the present work we are concerned with the following questions:

- Can natural gas be produced by depressurization through drilling a well into a hydrate reservoir?
- What are the parameters that control the natural gas production rate? In particular, is the gas production thermally controlled?

We used the combined models of Verigin et al. (1980) and Bondarev and Cherskiy as reported by Makogon (1997). In this model, the fluid energy equation is used to describe the temperature and pressure distributions of the natural gas in the porous layer. The conductive and convective heat transfer, as well as the effects of the throttling process were also included. Assuming the hydrate layer also contained pressurized natural gas, Makogon (1997) linearized the governing equations and obtained a set of self-similar solutions for temperature and pressure distributions in the reservoir. The results lead to a system of coupled algebraic equations for the location of the decomposition front, and the temperature and pressure at the front. The numerical simulation of the results, however, has not appeared in the literature (Makogon, 1998). In the present work, the corresponding system of algebraic equations (with minor corrections) is solved by an iterative scheme. For several well pressures and reservoir temperatures, numerical results for time evolution of pressure and temperature profiles in the hydrate reservoir, as well the location of the front and the natural gas production rate are obtained. The sensitivity of the natural gas production from hydrate by depressurization to

variations of reservoir parameters is studied. In particular, effects of reservoir porosity and permeability in both the gas and the hydrate regions on gas production rate and pressure and temperature distributions across the reservoir are studied. The results are presented in graphical form and discussed.

2. Hydrate decomposition model

In this study the decomposition of methane hydrate in a reservoir due to depressurization is considered. Chemical reaction of methane with water to from hydrate is represented by

$$(CH_4)_{gas} + 6(H_2O)_{water} \leftrightarrow (CH_4 \bullet 6H_2O)_{solid}.$$

When the pressure decreases or the temperature rises, the reaction reverses and the hydrate decomposes into CH_4 and water.

Suppose there is a large pressurized methane hydrate reservoir underground. It is assumed that solid hydrate and natural gas exist in the porous layer at the reservoir pressure P_e and reservoir temperature T_e. Hydrate is stable at this pressure and temperature at the initial time. When a well is drilled into the reservoir, the pressure in the well drops to a certain value $P_G < P_D < P_e$, where P_D is the decomposition pressure of the hydrate at the dissociation temperature, T_D. At this moment the hydrate near the well becomes unstable and begins to decompose into natural gas and water. The process of hydrate decomposition then expands outward with time. It is assumed that the hydrate decomposition in a porous medium does not occur in the entire volume, but in a certain narrow region which can be treated as a surface, the so-called decomposition front. This moving front separates the volume of the reservoir into two zones with different phases. In the near-well zone only natural gas and water exist, while in the zone further away from the well only the solid hydrate and natural gas exist. Pressures and temperatures in these two zones gradually decrease, and the natural gas moves towards the well because of the pressure gradient, while the decomposition front moves in the opposite direction.

It should be emphasized that the model proposed by Makogon (1997) and used in this study involves several important assumptions. One is that the pressure and temperature at any point on the decomposition front are the equilibrium pressure, P_D, and temperature, T_D, for dissociation of methane hydrate. Furthermore, the hydrate reservoir is assumed to be porous and contain natural gas. As the dissociation front moves outward, heat must be supplied to the front because of the endothermic nature of the hydrate decomposition process. Makogon (1997) suggested that heat conduction is negligible when compared with convection, and heat must be supplied from the reservoir for dissociation to continue. The other assumptions are that during hydrate decomposition the front is a source of mass that releases water and methane gas, the movement of water in the porous medium is negligible, and the permeability is constant.

3. Mathematical model

In this section, the mathematical formations suggested by Makogon (1997) are summarized. Consider a hydrate reservoir with a well as shown in Fig. 1. For a one-dimensional model the distribution of pressure in the layer is described using an analog of the classical Stefan's problem for melting:

$$\frac{2\Phi_n \mu}{k_n} \frac{\partial P_n}{\partial t} = \frac{\partial^2 P_n^2}{\partial x^2}, \tag{1}$$

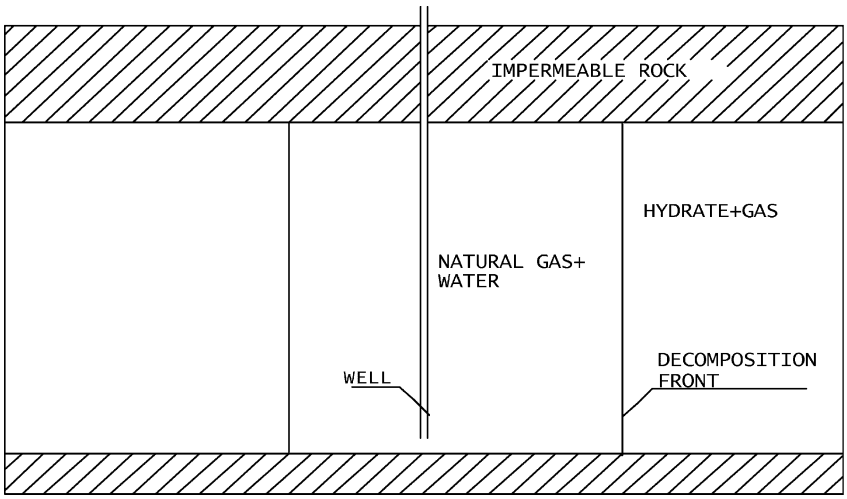

Fig. 1. Schematics of the hydrate reservoir for the one-dimensional model.

where

$$\Phi_1 = (1-\alpha)\Phi, \tag{2}$$

$$\Phi_2 = (1-\beta)\Phi, \tag{3}$$

where μ is viscosity of gas, k_n is gas permeability in zone 1 or 2, P_n is the pressure in zone 1 or 2, Φ is porosity, α is the water saturation, and β is the hydrate saturation. In Eq. (1) and in the subsequent analysis, $n=1$ corresponds to the region $0 < x < l(t)$, and $n=2$ to the region $l(t) < x < \infty$, where $l(t)$ is the distance of dissociation front from the origin (located at the well).

The boundary conditions are

$$P_1(0,t) = P_G, \qquad P_2(x,0) = P_2(\infty,t) = P_e, \tag{4}$$

$$P_1(l(t),t) = P_2(l(t),t) = P_D(T_D), \tag{5}$$

$$T_2(x,0) = T_2(\infty,t) = T_e, \tag{6}$$

$$T_1(l(t),t) = T_2(l(t),t), \tag{7}$$

where P_n is pressure in zone 1 or 2, T_n is temperature in zone 1 or 2, P_D is pressure at the decomposition front, and T_D is temperature at the front. As noted before, it is assumed that P_D and T_D are the equilibrium pressure and temperature for dissociation of methane hydrate.

The relation between temperature T_D and pressure P_D on the decomposition front in terms of the phase equilibrium between natural gas and hydrate is

$$\log_{10} P_D = a(T_D - T_0) + b(T_D - T_0)^2 + c, \tag{8}$$

where T_0 is 273.15 K and a, b, c are empirical constants that depend on the hydrate composition. Values of a, b, and c are obtained from the equilibrium pressure–temperature data of methane hydrate (Makogon, 1997). Using the least square fit method we get:

$$a = 0.0342/K, \qquad b = 0.0005/K^2, \qquad c = 6.4804,$$

where in Eq. (8) P_D is in Pa.

Fig. 2 compares the result of prediction of Eq. (8) with the data obtained by Marshall, Saito, and Kobayashi (1964). It is observed that the fit is in good agreement with the data in the range of variables considered.

The mass balance for gas at the decomposition front, $l(t)$, as obtained by Verigin et al. (1980) is

$$\rho_1 v_1 - \rho_2 v_2 = -[\beta\varepsilon\rho_3 - (1-\alpha)\rho_1 + (1-\beta)\rho_2]\Phi\frac{\mathrm{d}l}{\mathrm{d}t}, \tag{9}$$

where ρ_1 is the density of natural gas in zone 1, ρ_2 is the density of natural gas in zone 2, and ρ_3 is the density of hydrate, ε is the mass fraction of gas in methane hydrate. Here v_1 and v_2 are the velocities of natural gas in zones 1 and 2, and ε is the mass fraction of gas in the hydrate.

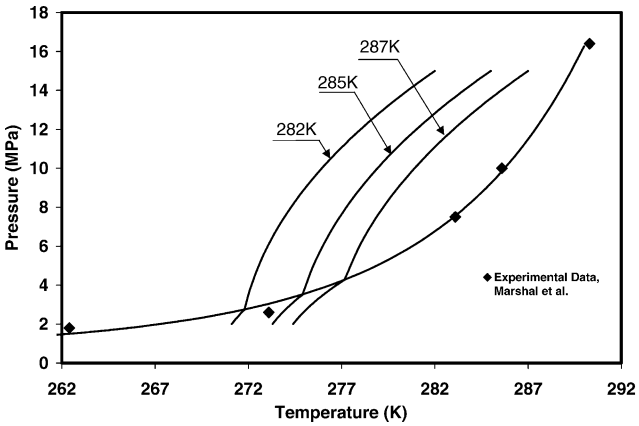

Fig. 2. Equilibrium of pressure–temperature of methane hydrate, and variations of P–T during the dissociation process for the well pressure of 2 MPa and reservoir pressure of 15 MPa with different reservoir temperatures.

The densities of the natural gas in zones 1 and 2 at the decomposition front are the same. i.e.,

$$\rho_1(l,t) = \rho_2(l,t) = \rho_0\frac{P_D T_0}{z P_0 T_D}, \tag{10}$$

where z is the gas compressibility, and ρ_0 is the gas density at atmospheric pressure P_0 and temperature T_0.

Substituting (10) into (9), it follows that:

$$v_1(l,t) - v_2(l,t) = -\left[\varepsilon\beta\frac{\rho_3 P_0 T_D}{\rho_0 P_D T_0} z - (\beta-\alpha)\right]\Phi\frac{\mathrm{d}l}{\mathrm{d}t}. \tag{11}$$

The mass balance equation for water is given as

$$\rho_W \Phi\alpha = (1-\varepsilon)\rho_3\Phi\beta, \tag{12}$$

where ρ_W is the density of water.

The temperature field of the gas-saturated layer is governed by the convective–conductive heat transfer equation that includes a temperature change because of throttling and adiabatic effects. i.e.,

$$a_n\frac{\partial^2 T_n}{\partial x^2} = \frac{\partial T_n}{\partial t} - \frac{c_v k_n}{c_n\mu}\frac{\partial P_n}{\partial x}\left(\frac{\partial T_n}{\partial x} - \delta\frac{\partial P_n}{\partial x}\right) - \eta\frac{\Phi_n c_v}{c_n}\frac{\partial P_n}{\partial t}, \tag{13}$$

where a_n is the heat diffusivity, c_n is the heat capacity, c_v is the constant volume heat capacity of gas, δ is the throttling coefficient, and η is the adiabatic coefficient of the gas. Note that the Joule–Thompson throttling process is accounted for in Eq. (13).

4. Linearization and self-similar solution

Using the approximation

$$\frac{\partial P_1^2}{\partial t} \approx 2P_G\frac{\partial P_1}{\partial t}, \qquad \frac{\partial P_2^2}{\partial t} \approx 2P_e\frac{\partial P_2}{\partial t}, \tag{14}$$

Eq. (1) may be linearized as

$$\frac{\partial P_n^2}{\partial t} = \chi_n \frac{\partial^2 P_n^2}{\partial x^2}, \tag{15}$$

where

$$\chi_1 = \frac{k_1 P_G}{\Phi(1-\alpha)\mu}, \qquad \chi_2 = \frac{k_2 P_e}{\Phi(1-\beta)\mu}. \tag{16}$$

Self-similar solutions of Eq. (15) with boundary conditions (4)–(7) as obtained by Makogon (1997) are given as

$$P_1^2 = P_G^2 - (P_G^2 - P_D^2)\frac{\operatorname{erf}\lambda_1}{\operatorname{erf}\alpha_1}, \tag{17}$$

$$P_2^2 = P_e^2 - (P_e^2 - P_D^2)\frac{\operatorname{erfc}\lambda_2}{\operatorname{erfc}\alpha_2}, \tag{18}$$

where

$$\lambda_n = \frac{x}{2\sqrt{\chi_n t}}, \qquad \alpha_n = \sqrt{\frac{\gamma}{4\chi_n}}, \tag{19}$$

$$l(t) = \sqrt{\gamma t}. \tag{20}$$

Here, γ is a constant (to be determined) and the error function and complementary error function are defined as

$$\operatorname{erf}(\xi) = \frac{2}{\sqrt{\pi}}\int_0^{\xi} \mathrm{e}^{-\eta^2}\,\mathrm{d}\eta, \qquad \operatorname{erfc}(\xi) = 1 - \operatorname{erf}(\xi). \tag{21}$$

Under the condition that the hydrate reservoir contains natural gas, neglecting the conductive heat transfer in the porous medium, which is much smaller than the convective heat transfer, Eq. (13) becomes:

$$\frac{\partial T_n}{\partial t} - \frac{c_v k_n}{c_n \mu}\frac{\partial P_n}{\partial x}\left(\frac{\partial T_n}{\partial x} - \delta\frac{\partial P_n}{\partial x}\right) - \eta\frac{\Phi_n c_v}{c_n}\frac{\partial P_n}{\partial t} = 0. \tag{22}$$

Solutions to the linearized form of Eq. (22) satisfying the boundary conditions (4)–(7) are given as (Makogon, 1997),

$$T_1 = T_D + A_1\delta\left[\operatorname{erf}\lambda_1 - \operatorname{erf}\alpha_1 + \left(\frac{\eta}{\delta}B_1 - 1\right)\left(\Psi_1(\lambda_1) - \Psi_1(\alpha_1)\right)\right], \tag{23}$$

$$T_2 = T_e - A_2\delta\left[\operatorname{erfc}\lambda_2 + \left(\frac{\eta}{\delta}B_2 - 1\right)\Psi_2(\lambda_2)\right], \tag{24}$$

where

$$\Psi_1(\xi_1) = \frac{2}{\sqrt{\pi}}\int_0^{\xi_1}\frac{\eta\mathrm{e}^{-\eta^2}}{\eta + C_1\mathrm{e}^{-\eta^2}}\,\mathrm{d}\eta,$$

$$\Psi_2(\xi_2) = \frac{2}{\sqrt{\pi}}\int_{\xi_2}^{\infty}\frac{\eta\mathrm{e}^{-\eta^2}}{\eta + C_2\mathrm{e}^{-\eta^2}}\,\mathrm{d}\eta, \tag{25}$$

$$A_1 = \frac{1}{2\operatorname{erf}\alpha_1}\frac{P_D^2 - P_G^2}{P_G}, \qquad A_2 = \frac{1}{2\operatorname{erfc}\alpha_2}\frac{P_e^2 - P_D^2}{P_e}, \tag{26}$$

$$B_1 = \frac{\Phi_1 c_v}{c_1}, \qquad B_2\frac{\Phi_2 c_v}{c_2}, \tag{27}$$

$$C_1 = \frac{P_D^2 - P_G^2}{P_G}\frac{c_v}{c_1}\frac{1}{2\sqrt{\pi}\operatorname{erf}\alpha_1}\frac{k_1}{\mu\chi_1},$$

$$C_2 = \frac{P_e^2 - P_D^2}{P_e}\frac{c_v}{c_2}\frac{1}{2\sqrt{\pi}\operatorname{erfc}\alpha_2}\frac{k_2}{\mu\chi_2}. \tag{28}$$

The values of pressure P_D and temperature T_D at the decomposition front, and the constant γ, which determines the motion of the decomposition front, are still unknown and must be evaluated numerically for given set of conditions. From the evaluation of Eq. (24) at the decomposition front (i.e. $\lambda_2 = \alpha_2$), it followed that:

$$T_D = T_e - A_2\delta\left[\operatorname{erfc}\alpha_2 + \left(\frac{\eta}{\delta}B_2 - 1\right)\Psi_2(\alpha_2)\right]. \tag{29}$$

The equilibrium pressure P_D and the equilibrium temperature T_D are related through Eq. (8). Substitute Eqs. (17) and (18) into Eq. (11), we obtain the equation for determining the constant γ. i.e.,

$$k_1\frac{P_D^2 - P_G^2}{\sqrt{\pi\chi_1}}\frac{\mathrm{e}^{-\alpha_1^2}}{\operatorname{erf}\alpha_1} - k_2\frac{P_e^2 - P_D^2}{\sqrt{\pi\chi_2}}\frac{\mathrm{e}^{-\alpha_2^2}}{\operatorname{erfc}\alpha_2} = A\sqrt{\gamma}, \tag{30}$$

where

$$A = \left[\varepsilon\beta\frac{\rho_3 P_0 T_D}{\rho_0 T_0}z - (\beta - \alpha)P_D\right]\Phi\mu. \tag{31}$$

Eqs. (8), (29) and (30) are three non-linear coupled equations for determining γ, T_D and P_D. An iterative scheme is used for evaluating the numerical values of these parameters. It is important to note that in this model the resulting dissociation pressure and temperature are fixed and depend only on the well pressure, and the reservoir pressure and temperature. The production rate of methane gas per unit length of the well is then given as

$$Q = \frac{k_1}{\mu}\frac{\partial P_1(0,t)}{\partial x} = \frac{k_1}{\mu}\frac{P_D^2 - P_G^2}{P_G}\frac{1}{\operatorname{erf}\alpha_1}\frac{1}{2\sqrt{\pi\chi_1 t}}. \tag{32}$$

Eq. (32) clearly shows that the well production rate decreases inversely with the square root of time, and increases with reservoir permeability.

It should be noted here that the linearization model suggested by Makogon (1997) and used in here neglects the heat conduction in the entire reservoir. Thus, the energy balance at the dissociation front cannot be enforced. While this is a limitation of the approach, many features of the hydrate reservoir behavior can be examined using the linearized solutions.

Table 1
Values of dissociating temperature and pressure and parameter γ for given reservoir and well conditions

P_e (MPa)	T_e (K)	P_G (MPa)	T_D (K)	P_D (MPa)	γ (m^2/s)
15	280	2	270.07	2.42	0.00012
15	285	2	275.44	3.69	0.00048
15	287	2	277.66	4.47	0.00125
15	287	3	277.69	4.49	0.00067
15	287	4	277.93	4.58	0.00015
15	287	4.53	278.04	4.64	0.000002

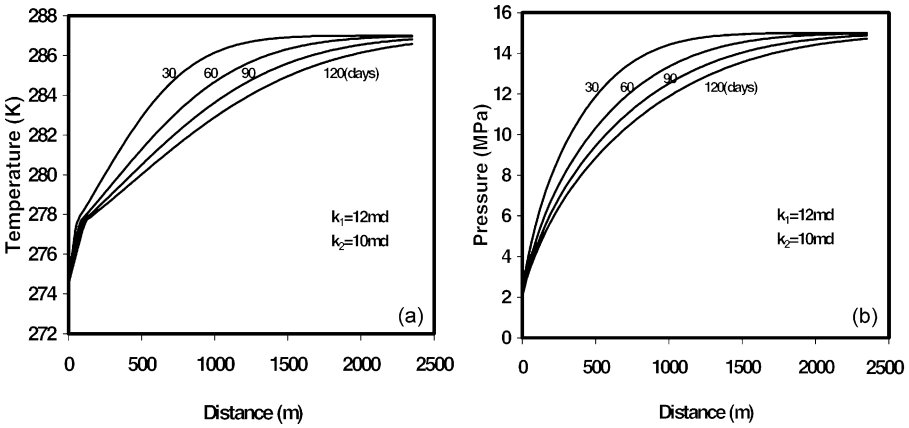

Fig. 3. Time variations of pressure and temperature in the reservoir for a well pressure of 2 MPa and a reservoir temperature of 287 K.

5. Results

This section presents numerical results for the time evolution of pressure and temperature profiles in a hydrate reservoir under various conditions. In addition, time variations of methane gas production, and location of the dissociation front are also evaluated. A set of parametric study is performed and the sensitivity of natural gas production to various reservoir parameters is discussed. Unless stated otherwise, the conditions listed in notation and an initial reservoir pressure of 15 MPa are used in the simulation.

5.1. Well pressure and reservoir temperature

For different values of well pressure and initial reservoir temperature, the solutions to Eqs. (8), (29) and (30) are obtained. The resulting values of dissociating temperature and pressure at the front and the parameter γ with an error bound of 0.1% are listed in Table 1.

For given reservoir pressure and temperature and well pressure, the present linearized one-dimensional model leads to fixed values of dissociation-front pressure and temperature. Table 1 also shows that when the well pressure changes, the dissociation pressure and temperature change only slightly. The value of parameter γ, which controls the movement of the front and the gas production rate, decreases sharply with increase of well pressure. The dissociation pressure and temperature are, however, sensitive functions of reservoir temperature. A decrease of 2 K in the reservoir temperature drops the dissociation pressure by about 0.8 MPa, and reduces parameter γ by about 62%. An additional 5 K drop in the reservoir temperature leads to a reduction of dissociation pressure by about 1.2 MPa and reduces γ by a factor of 6.5.

For a well pressure of 2 MPa, Fig. 3 shows variations of reservoir pressure and temperature at different times. As noted before, the hydrate reservoir is divided into two zones by the decomposition front, and the temperature variations in the two zones are quite different. Fig. 3a shows that the temperature decreases gradually from the undisturbed reservoir value far from the front to the decomposition temperature at the front. The temperature gradient in the hydrate zone is largest near the front. In the gas zone, the temperature varies sharply and decreases to its minimum value at the well. The temperature profiles in the hydrate and the gas zones are also self-similar, and evolve with time as the decomposition front moves outward.

The corresponding pressure profiles for different times under the same conditions of Fig. 3a are presented in Fig. 3b. The pressure decreases gradually from the reservoir pressure to the decomposition pressure at the front, and then decreases toward the well to its minimum value at the well. For the present assumed condition that the zone permeabilities in the hydrate and the gas region are

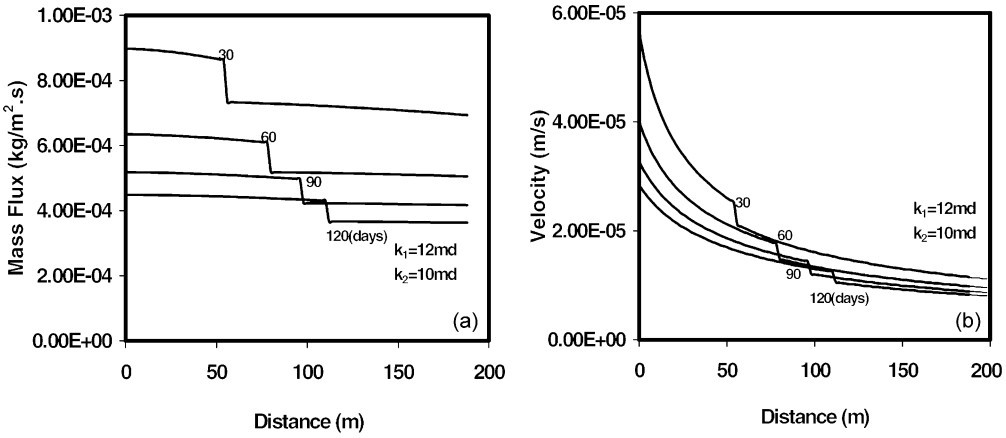

Fig. 4. Mass flux and velocity profiles for a reservoir temperature of 287 K and a well pressure of 2 MPa.

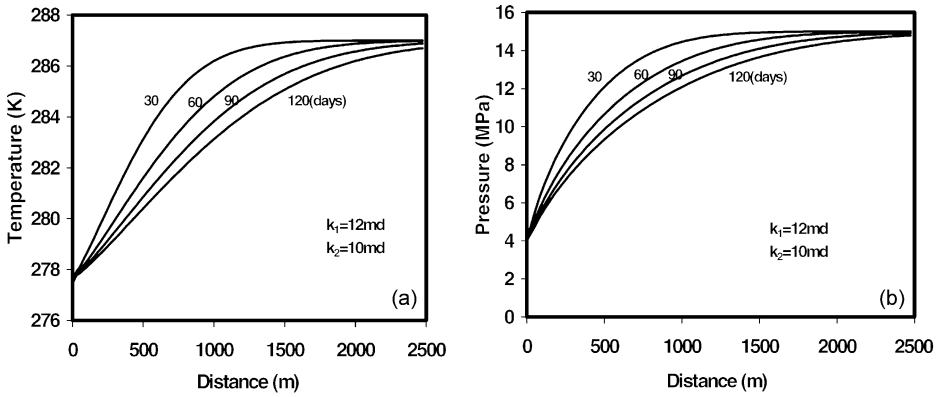

Fig. 5. Time variations of temperature and pressure in the reservoir for a well pressure of 4 MPa and a reservoir temperature of 287 K.

comparable, the change of slope of the pressure profile at the front is hardly noticeable. For the case that the permeability in the gas zone is much larger than that in the hydrate zone, Ahmadi, Ji, and Smith (2000) reported a significant change of slope of the pressure profile at the decomposition front. Fig. 3b also shows that the pressure profiles for different times are self-similar in each zone, and expand outward as the decomposition front moves away from the well.

Fig. 4 shows time evolutions of gas mass flux (in kg/m^2s) and gas velocity (in m/s) across the reservoir for a well pressure of 2 MPa. Fig. 4a shows that there is a jump in the mass flux due to hydrate dissociation at the front. The jump moves outward with time as the decomposition front penetrates deeper into the hydrate reservoir. It is also noticed that for the one-dimension model, the gas mass flux in the reservoir and the amount of natural gas generated due to hydrate dissociation decrease with time. Fig. 4b shows the time variation of natural gas velocity toward the well. It is seen that the gas velocity varies significantly across the reservoir. Natural gas velocity increases towards the well and a velocity jump at the decomposition front.

Fig. 5 shows the pressure and temperature profiles for a well pressure of 4 MPa. The reservoir pressure and temperature are kept constant at 15 MPa and 287 K. Except for the slower movement of the front, variations of pressure and temperature profiles in this figure are quite similar to those shown in Figs. 3. Fig. 5 shows that the dissociation front is at about 30 m after 120 days. In comparison, for a well pressure of 2 MPa, the front would be at 110 m under the same conditions. In the hydrate zone, the pressure and temperature decrease from their reservoir values at large distances to the dissociation values at the front. Other features of pressure and temperature profiles in the hydrate zone are quite similar to those for lower well pressures. Comparatively, large gradients occur near the front on the hydrate side. The pressure and temperature in the gas region then decrease rather sharply toward their minimum values at the well. For the well pressure of 4 MPa, the dissociation pressure and temperature at the front become close to the well pressure and temperature.

Fig. 6 shows variations of non-dimensional temperature and pressure profiles versus the similarity variable λ_1 as given by Eqs. (17), (18), (23) and (24). Here the

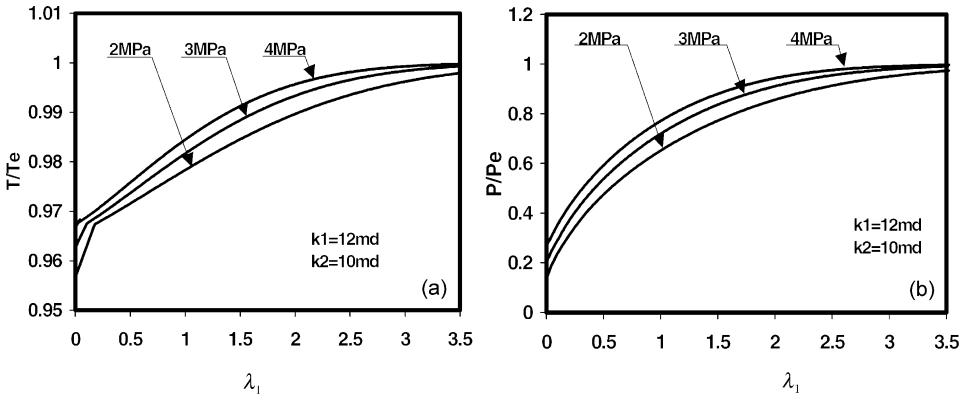

Fig. 6. Non-dimensional temperature and pressure profiles versus similarity variable λ_1 for different well pressures for a reservoir temperature of 287 K and a reservoir pressure of 15 MPa.

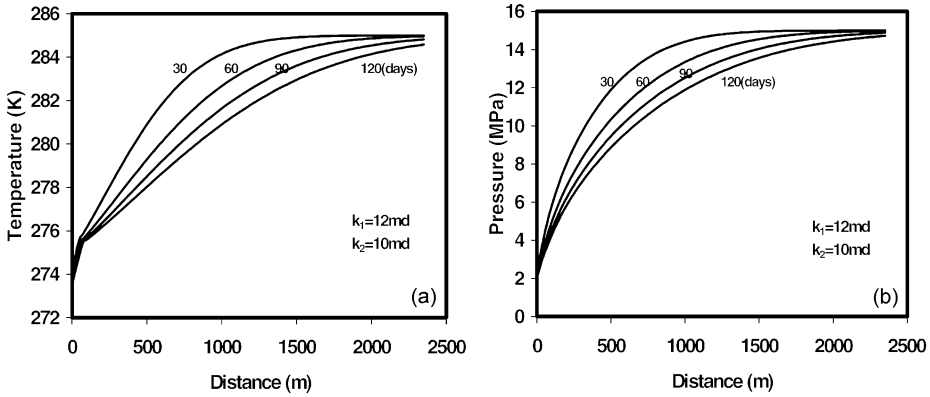

Fig. 7. Time variations of pressure and temperature in the reservoir for a well pressure of 2 MPa and a reservoir temperature of 285 K.

temperature and pressure are normalized with respect to the undisturbed reservoir conditions. While the general features of the similarity profiles are comparable, it is seen that the well pressure noticeably affects the variation of temperature and pressure profiles. At a high well pressure, the pressure and temperature profiles approach their saturation values for smaller values of λ_1, and the gas zone is comparatively small. For low well pressure, the saturation values are approached at higher values of $\lambda_1$and the gas zone is comparatively large.

For the case that the well pressure is 2 MPa, but the reservoir temperature is 285 K (2 K lower that the case shown in Fig. 3), the pressure and temperature profiles are presented in Fig. 7. While these profiles are quite similar to those shown in Figs. 3, the decomposition pressure and temperature are noticeably smaller. The movement of the front also markedly slows down for this lower-temperature reservoir. This observation further emphasizes the importance of heat transfer in hydrate dissociation and production processes. In the present one-dimensional model, the heat required for hydrate dissociation must be supplied by the hydrate reservoir. Therefore, the reservoir temperature becomes an important controlling parameter. (It should be emphasized that, for natural hydrate reservoirs, heat could also be transferred form the sides, which would significantly affect the natural gas production process.)

Mass flux and velocity profiles for a reservoir temperature of 285 K and a well pressure of 2 MPa are shown in Fig. 8. The other reservoir conditions are kept unchanged. Variations of the mass flux and velocity profiles are similar to those shown in Fig. 4 for a higher reservoir temperature. The main difference is that the mass flux and velocity jumps in Fig. 8 occur at a shorter distance from the well. The well output (gas velocity and mass flux), however, reduces as the reservoir temperature reduces.

Fig. 9a shows the movement of the decomposition front for different well pressures. Here the reservoir conditions are kept fixed at 15 MPa and 287 K. As expected, the distance of the front from the well increases proportional to the square root of time. As the well pressure increases, the motion of the front decreases, especially as the well pressure approaches the decomposition pressure.

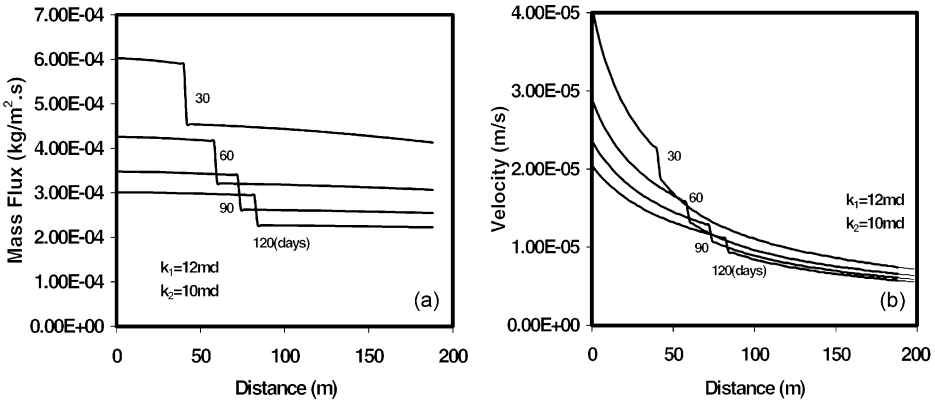

Fig. 8. Mass flux and velocity profiles for a reservoir temperature of 285 K and a well pressure of 2 MPa.

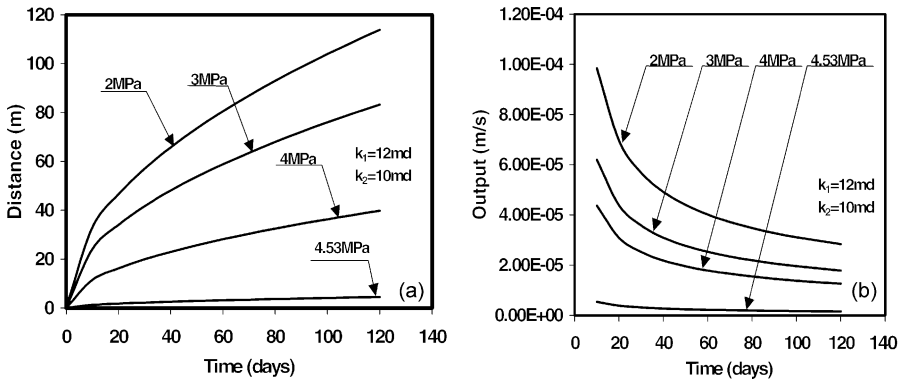

Fig. 9. Time variations of distance of decomposition front and natural gas output for a reservoir temperature of 287 K and for different well pressures.

Fig. 9b shows time variations of natural gas flow rate per unit height (and per unit width) of the well for different well pressures. As expected the flow rate decreases with inverse square root of time. For fixed reservoir conditions, the well output is a sensitive function of well pressure, and the production rate decreases sharply as the well pressure increases.

It is perhaps of interest to compare the simulated natural gas production rate with the recorded data from natural hydrate reservoirs. Makogon (1997) reported that in Messoyakhi field the natural gas production rate ranged from 5000 to 20,000 m^3/day for a well pressure of 0.2 MPa before inhibitor injection. The thickness of hydrate zone in this field was estimated to be 25 m. While there have been questions about the contribution of hydrate dissociation to the natural gas production in Messoyakhi field, it is the only reported field data currently available. Fig. 9b shows that the predicted natural gas production rate is of the order of 10^{-4} m^3/s per 1 m^2 of well, for a well pressure of 2 MPa. This is about 173 m^3/day per 1 m^2 of well for an atmospheric well pressure. Considering the differences in the reservoir permeability and other parameters, the simulated gas production rates in Fig. 9b appear to be in the range of the observation for the Messoyakhi field.

For fixed reservoir and well pressures, time evolutions of decomposition front and the well production rate for different reservoir temperatures are shown in Fig. 10. It is observed that the reservoir temperature significantly affects the motion of the front and the well output. When the reservoir temperature decreases by about 2–7 K, the distance of the dissociation front from the well decreases by about 30–80%, and the well output decreases by about 30–90%.

6. Sensitivity analysis

This section presents sensitivity analysis results for time evolutions of pressure and temperature profiles in a hydrate reservoir for a range of parameters. Time variations of methane gas production and location of the dissociation front are also evaluated. As noted before, it is assumed that the entire hydrate reservoir is porous and contains pressurized natural gas, and the hydrate saturation is less than 0.25.

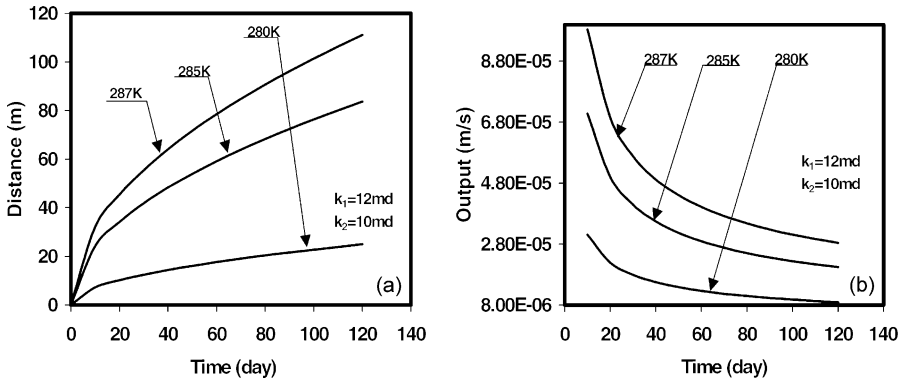

Fig. 10. Time variations of the distance of decomposition front and the natural gas output for a well pressure of 2 MPa and for different reservoir temperatures.

Table 2
Values of dissociating temperature and pressure and parameter γ for different zone permeabilities

P_e (MPa)	T_e (K)	P_G (MPa)	k_1 (md)	k_2 (md)	T_D (K)	P_D (MPa)	γ (m^2/s)
15	287	2	1.2	0.2	277.42	4.38	0.0003
15	287	2	6	3	277.64	4.45	0.00087
15	287	2	12	10	277.66	4.47	0.00125
15	287	2	120	10	277.32	4.34	0.0384

6.1. Zone permeability

Zone permeabilities are important reservoir parameters that could affect the natural gas production. In this section, variations of natural gas production rate, as well as the reservoir pressure and temperature profiles for different permeabilities, are studied. We expect the relative permeability for the gas in the gas zone to be somewhat larger than that in the hydrate zone. In the simulation, however, a wide range of values is used to clearly show the sensitivity of the result to zone permeability.

Table 2 lists the computed values of dissociation temperature and pressure at the front and the parameter γ for different values of the zone permeabilities. Here, the porosity and hydrate saturation are kept fixed at $\Phi = 0.2$ and $\beta = 0.19$, and the other reservoir conditions are listed in notation. It should be emphasized that permeability and porosity are usually related and keeping the porosity fixed in these simulations is an idealization. (Sensitivity to variation of porosity when permeability is a function of porosity is studied in the next section.) Table 2 shows that when the zone permeability changes, the dissociation pressure and temperature change only slightly. The value of parameter γ, however, decreases sharply as zone permeability decreases.

For different permeabilities, Fig. 11a shows time variations of the decomposition front movement. As expected, the decomposition front moves more slowly as the gas zone permeability becomes smaller. As noted before, this is because the distance of the front from the well is proportional to the parameter γ, which decreases as the gas zone permeability decreases.

Time variations of the well natural gas output (flow rate per unit height and per unit width) for different zone permeabilities are presented in Fig. 11b. It is noticed that the production rate decreases with time. (This is the consequence of the present one-dimensional model.) Fig. 11b also shows that the flow rate decreases as the zone permeabilities decrease.

Fig. 12 compares time variations of the temperature and pressure profiles for different permeabilities. It is seen that the reservoir cools down with time and the temperature profiles are self-similar. Furthermore, the decomposition front moves faster into the reservoir as zone permeabilities increase; thus, the reservoir temperature decreases as zone permeabilities increase. Also, the temperature gradient in the gas zone decreases, while the temperature gradient in the hydrate zone increases, as the hydrate zone permeability increases.

For the same reservoir conditions, Figs. 12b and d show time variations of pressure profiles for different permeabilities. The pressure in the hydrate zone drops to the dissociation pressure with a rather sharp gradient near the dissociation front. The pressure then decreases to the well pressure with a slope that is a sensitive function of zone permeability in the hydrate region. The pressure gradient in the gas zone decreases as the permeability increases. A similar trend was also observed by Ahmadi et al. (2000).

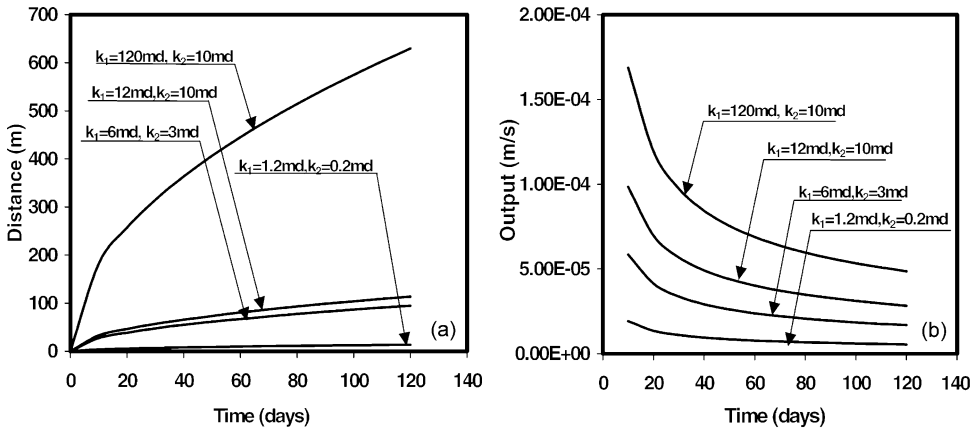

Fig. 11. Variations of distance of decomposition front and natural gas output for a well pressure of 2 MPa and a reservoir temperature of 287 K for different permeabilities.

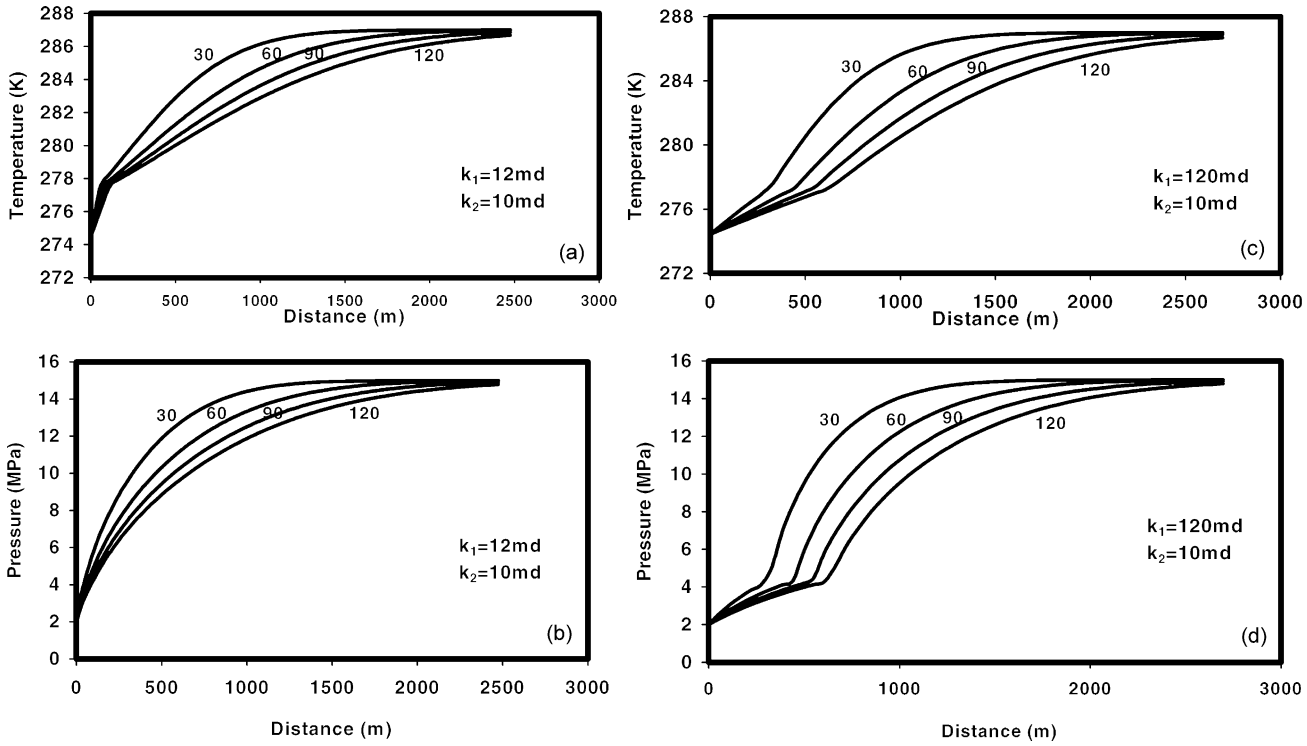

Fig. 12. Comparison of temperature and pressure profiles for different permeabilities for a well pressure of 2 MPa and a reservoir temperature of 287 K.

6.2. *Reservoir porosity*

Another important parameter is the porosity of the hydrate reservoir. As was noted before, permeability is a strong function of porosity. Sensitivity of natural gas production to variations in reservoir porosity is studied in this section. In this case, the hydrate saturation is kept fixed at $\beta = 0.19$, but zone permeabilities are allowed to change as a function of porosity. According to the Kozeny–Carman equation (Kaviani, 1995),

$$k_i \sim \Phi^3, \tag{33}$$

where k_i is the zone permeability and Φ is the porosity. Thus as Φ changes, the zone permeabilities must be adjusted according to Eq. (33) for consistency. The other reservoir conditions as listed in notation are kept fixed. Table 3 lists the resulting values of dissociation temperature and pressure at the front and the parameter γ for the

Table 3
Values of dissociating temperature and pressure and parameter γ for different reservoir porosities

P_e	T_e (K)	P_G (MPa)	k_1 (md)	k_2 (md)	Φ	T_D (K)	P_D (MPa)	γ (m^2/s)
15	287	2	12	10	0.2	277.66	4.47	0.00125
15	287	2	40.5	33.75	0.3	273.80	3.22	0.000492
15	287	2	96	80	0.4	270.84	2.56	0.000148

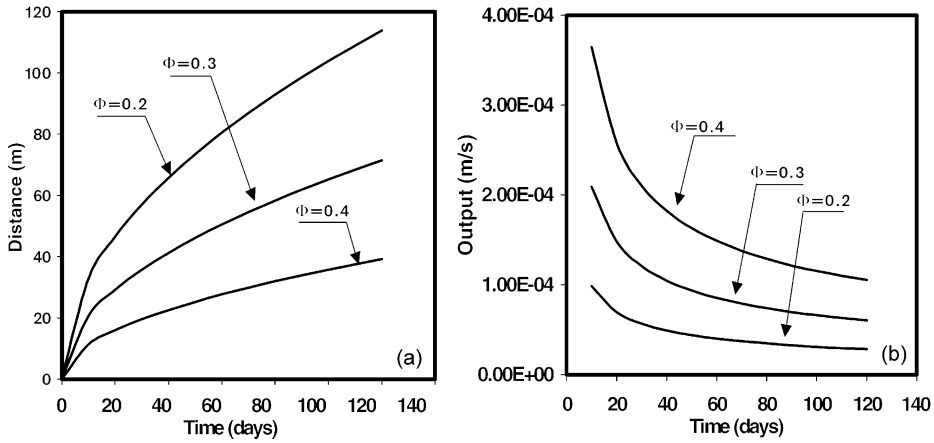

Fig. 13. Variations of distance of decomposition front and natural gas output for a well pressure of 2 MPa and a reservoir temperature of 287 K for different porosities.

different porosities. This table shows that the dissociation pressure and temperature, as well as the parameter γ are all sensitive functions of porosity. As porosity increases, and as a result k_1 and k_2 increase, T_D, P_D, and γ, decrease sharply.

For different porosities, Fig. 13a shows time variations of the decomposition front movement. It is observed that the increase of porosity and permeabilities makes the decomposition front move more slowly, although the gas output increases. Time variations of natural gas output (flow rate per unit height per unit width of the well) are shown in Fig. 13b for different porosities. As expected the flow rate increases as the reservoir porosity increases. This is because with the increase of reservoir porosity, the zone permeabilities increase and also there is larger amount of hydrate available to dissociate.

Fig. 14 compares temperature and pressure profiles at different times for different reservoir porosities. With the increase of porosity, the decomposition front move more slowly and both the hydrate and gas zone temperatures decrease. The pressure profiles are similar, but the magnitude of pressure decreases as Φ increases.

7. Conclusions

Natural gas production from decomposition of methane hydrate in confined, pressurized reservoirs is studied. Evolutions of pressure and temperature profiles in one-dimensional reservoirs are analyzed, and the effects of variation in well pressure and reservoir temperature are studied. The sensitivity of natural gas production from hydrate to variations in reservoir parameters such as porosity and permeability is also studied. Time evolutions of pressure and temperature profiles across the reservoir, as well as the movements of decomposition front, are analyzed. On the basis of the results presented, the following conclusions are drawn:

1. Under favorable conditions natural gas can be produced from hydrate reservoirs by a depressurization well.
2. The reservoir physical and thermal conditions and the well pressure control the natural gas production rate.
3. While the hydrate dissociation is thermally controlled, for a reservoir with hydrate in the pores, the required heat could be supplied by the natural gas convection from the far field.
4. For an infinite homogenous hydrate reservoir containing natural gas, the dissociation pressure and temperature are fixed (with in the bound of a linearized model), and depend only on the reservoir conditions and the well pressure.
5. For a fixed reservoir pressure and temperature, the well output decreases and the motion of the decomposition front slows as the well pressure increases.

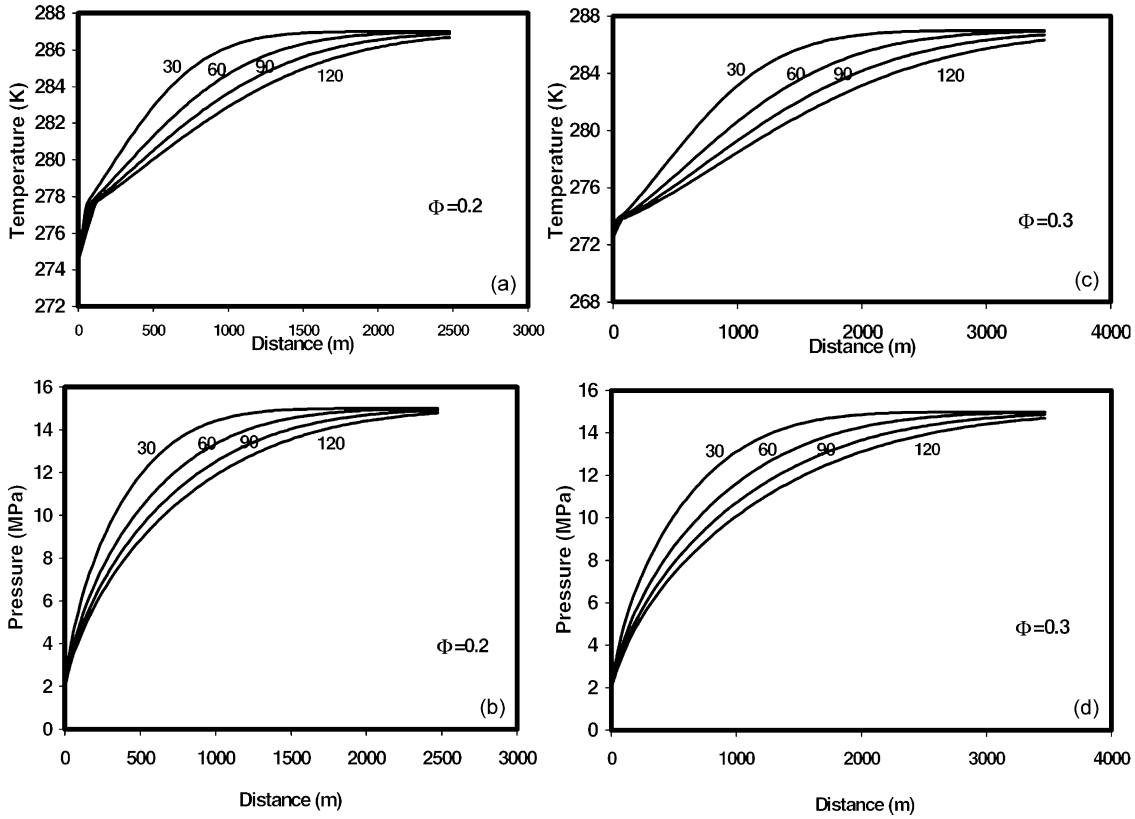

Fig. 14. Comparison of temperature and pressure profiles for different porosities for a well pressure of 2 MPa and a reservoir temperature of 287 K.

6. For fixed reservoir and well pressures, the gas production rate decreases significantly as the reservoir temperature decreases.
7. For this model, the distance of the decomposition front from the well increases in direct proportion to the square root of time, and the production rate decreases in inverse proportion.
8. For a homogenous hydrate reservoir, the reservoir permeability significantly affects the rate of convective heat transfer and consequently the rate of natural gas production.
9. For a fixed porosity, the reservoir with higher permeability has higher production rate and the decomposition front penetrates faster into the reservoir. The variation of permeability, however, has a slight effect on the dissociation temperature and pressure at the front.
10. When permeability is related to porosity through the Koznery–Carman type equation, the natural gas output and the motion of the decomposition front are sensitive functions of the reservoir porosity. The variation of reservoir porosity also alters the dissociation temperature and pressure to a noticeable extent. As porosity increases, gas output increases, and the decomposition pressure and temperature decrease. The speed of decomposition front motion, however, decreases.

As noted before, the presented linearization model that neglects the heat conduction in the entire reservoir cannot enforce the balance of energy at the dissociation front. Removing this limitation that requires numerical solution of the original nonlinear equations will be reported in a future communication.

Notation

a, b, c	empirical constants in Eq. (8)
a	0.0342/K
b	0.0005/K^2
c	6.4804
a_n	thermal diffusivity of zones, m^2/s
c_v	volume heat capacity of gas (3000 J/K Kg)
c_1	heat capacity of zone 1 (2400.2 J/K Kg)
c_2	heat capacity of zone 2 (1030.2 J/K Kg)
k_1	phase permeability of gas in zone 1 (12 md)
k_2	phase permeability of gas in zone 2 (10 md)
l	the distance of decomposition front away from the well
t	time
v_1	velocity of natural gas in zone 1
v_2	velocity of natural gas in zone 2
x	distance
z	compressibility of gas (0.88)

P_0 atmospheric pressure (1.01×10^5 Pa)
P_D hydrate decomposition pressure
P_e reservoir pressure at initial time (15 MPa)
P_G pressure at the well, MPa
P_n pressure in zone 1 or 2
Q gas production rate per unit length of well
T_D hydrate decomposition temperature, K
T_e reservoir temperature at initial time, K
T_n temperature in zone 1 or 2
T_0 reference temperature (273.15 K)

Greek letters

α water content of pores (0.15)
β hydrate saturation of a layer (0.19)
γ constant related to movement of decomposition front
δ throttling coefficient of gas (8×10^{-7} K/Pa)
ε mass fraction of gas in methane hydrate (0.129)
η adiabatic coefficient of gas (3.2×10^{-6} K/Pa)
μ viscosity of gas (methane) (1.5×10^{-5} Pa S)
ρ_0 density of methane gas at atmospheric pressure P_0 and temperature T_0. (0.706 kg/m^3)
ρ_3 density of hydrate (0.91×10^3 kg/m^3)
ρ_W density of water (1.0×10^3 kg/m^3)
Φ porosity (0.2)
Φ_1 $(1-\alpha)\Phi$, content of free gas at zone 1
Φ_2 $(1-\beta)\Phi$, content of free gas at zone 2

Acknowledgements

The support of the Office of Fossil Energy, US Department of Energy and Clarkson University is gratefully acknowledged. The work of GA was also supported by a grant form US Department of Energy.

References

AGU, (1999). American Geophysical Union, Mineralogical Society of America, and Geochemical Society, Spring Meeting, Boston, MA, June 1–4.

Ahmadi, G., Ji, C., & Smith, D. H. (2000). A simple model for natural gas production from hydrate decomposition. In G. D. Holder, & P. R. Bishnoi (Eds.), *Gas hydrates: Challenges for the future*, Vol. 912 (pp. 420–427). New York: New York Academy of Sciences.

Burshears, M., O'Brien, T. J., & Malone, R. D. (1986). A multi-phase, multi-dimensional, variable composition simulation of gas production from a conventional gas reservoir in contact with hydrates, *Proceedings of Unconventional Gas Technology Symposium*, Louisville, KY, May 18–21, Society of Petroleum Engineers, SPE Paper 15246.

Durgut, I., & Parlaktuna, M. (1996). A numerical method for the gas production process in gas hydrate reservoirs. *Proceedings of the Second International Conference on Natural Gas Hydrates*, Toulouse, France, June 2–6.

Holder, G. D., Angert, P. F., & Godbole, S. P. (1982). Simulation of gas production from a reservoir containing both gas hydrates and free natural gas. *Proceedings of 57th Society of Petroleum Engineers Technology Conference*, New Orleans, September 26–29, SPE Paper 11005.

Kamath, V. (1983). *Study of heat transfer characteristics during dissociation of gas hydrates in porous media*. Ph.D. Thesis, University of Pittsburgh, Pittsburgh, PA.

Kaviani, M. (1995). *Principle of heat transfer in porous media*. New York: Springer.

Kim, H. C., Bishnoi, P. R., Heidemann, R. A., & Rizvi, S. S. H. (1987). Kinetics of methane hydrate decomposition. *Chemical Engineering Science*, *42*, 1645–1653.

Lysne, D. (1994). Hydrate plug dissociation by pressure reduction. In E. D. Sloan Jr., J. Happel, & M. A. Hnatow (Eds.), *International Conference on Natural Gas Hydrates*, Vol. 715 (pp. 714–717). New York: Academy of Science.

Makogon, Y. F. (1974). *Hydrates of natural gas* (Translated form Russian by Cieslesicz, W.J.) Tulsa, OK: Penn Well.

Makogon, Y. F. (1997). *Hydrates of hydrocarbons*. Tulsa, OK: Penn Well.

Makogon, Y. F. (1998). Private communication.

Marshall, D. R., Saito, S., & Kobayashi, R. (1964). Hydrates at high pressure: Part I, methane–water, argon–water, and nitrogen–water systems. *A.I.Ch.E. Journal*, *10*, 202–205.

Masuda, Y., Fujinaga, Y., Naganawa, S., Fujita, K., Sato, K., & Hayashi, Y. (1999). Modeling and experimental studies on dissociation of methane gas hydrates in berea sandstone cores. *Proceedings of the Third International Conference on Natural Gas Hydrates*, Salt Lake City, UT, July 18–22.

Moridis, G., Apps, J., Pruess, K., & Myer, L. (1998). EOSHYDR: A TOUGH2 module for CH_4-hydrate release and flow in the subsurface. LBNL-42386, Lawrence Berkeley National Laboratory, Berkeley, CA.

Selim, M. S., & Sloan, E. D. (1989). Heat and mass transfer during the dissociation of hydrates in porous media. *A.I.Ch.E. Journal*, *35*, 1049–1052.

Sloan Jr., E. D. (1998). *Clathrate hydrates of natural gases* (2nd ed). New York: Marcel Dekker.

Swinkels, W. J. A. M., & Drenth, R. J. J. (1999). Thermal reservoir simulation model of production from naturally occuring gas hydrate accumulations. *Proceedings 1999 SPE Annual Technical Conference*, Houston, TX, October 1999, SPE Paper 56550.

Tsypkin, G. (2000). Mathematical models of gas hydrates dissociation in porous media. In G. D. Holder, & P. R. Bishnoi (Eds.), *Gas hydrates: Challenges for the future*, Vol. 912 (pp. 428–436). New York: New York Academy of Sciences.

Verigin, N. N., Khabibullin, I. L., & Khalikov, G. A. (1980). Izvestiya Akademii NaukSSSR, Mekhanika Zhidkosti Gaza. No. 1, p. 174.